Electroreflectance of $Cu_2(Cd_{1-x}, Zn_x)SnS_4$ thin film solar cells

S. Levcenko,[1,2,*] S. S. Hadke,[3,4] L. H. Wong,[3,4] and T. Unold[2]

[1]*Felix-Bloch-Institut für Festkörperphysik, Universität Leipzig, Linnéstraße 5, 04103, Leipzig, Germany*

[2]*Department of Structure and Dynamics of Energy Materials, Helmholtz-Zentrum fur Materialien und Energie, Berlin 14109, Germany*

[3]*School of Materials Science and Engineering, Nanyang Technological University, Singapore 639798, Singapore*

[4]*Campus for Research Excellence and Technological Enterprise (CREATE), 1 Create Way, 139602, Singapore*

(Received 31 May 2021; accepted 10 September 2021; published 14 October 2021)

The effect of Cu off-stoichiometry and Zn alloying on the fundamental absorption region of Cu_2CdSnS_4 (CCTS) absorbers in complete solar cells has been investigated using electroreflectance (ER) spectroscopy at room temperature. It is found that ER spectra consist of contributions from two different sources, one of which corresponds to band gap transition in the absorber layer and the other to the interference effect in the window layer. ER measurements on CCTS samples reveal a near-constant band gap energy of 1.37–1.38 eV and a relatively small broadening of 60–90 meV in the probed $0.8 < Cu/(Cd + Sn) < 0.89$ compositional range, in contrast to related kesterites $Cu_2ZnSn(S, Se)_4$. The analysis of the band gap in $Cu_2(Cd_{1-x}, Zn_x)SnS_4$ alloys yields a quadratic dependence on Zn content with a bowing parameter of 0.4 eV. Finally, the broadening parameters of the band gap transitions as well as their compositional dependence are evaluated and discussed.

DOI: 10.1103/PhysRevMaterials.5.104605

I. INTRODUCTION

In recent years stannite Cu_2CdSnS_4 (CCTS) semiconductor has gained a renewed interest in thin film photovoltaic devices [1–3]. It has been known since the late 1970s, when the first single-crystal *p*-CCTS/*n*-CdS heterodiode with power conversion efficiency of 1.6% was demonstrated [4]. Nowadays, the solar cells made out of polycrystalline CCTS thin films reach efficiencies of about 8%, which is the highest result among fully cation-substituted absorbers derived from kesterite Cu_2ZnSnS_4 (CZTS) [5]. It has been also found that Cd alloying effectively suppresses the structural disorder of the kesterite CZTS as evidenced from the smaller band tailing and Urbach energy [2,6] and causes a phase transition to the stannite lattice in related $Cu_2(Cd_{1-x}, Zn_x)SnS_4$ (CCZTS) alloys [1,3]. Furthermore, the efficiency of CCZTS-based solar cells has approached or exceeded 12% in recent years [2,7]. However, not very much is known about the electronic band structure of CCZTS alloys in comparison to an extensively studied kesterite $Cu_2ZnSn(S, Se)_4$ family of materials [8,9]. For example, the experimentally obtained band gap of CCTS spans from ∼1.1 eV [10,11] to ∼1.4 eV [1,4] and there is some discrepancy between the reported band gap dependency on alloy composition in CCZTS [1,3,11]. The absorption measurements on CCZTS deduced a linear band gap variation from 1.09 to 1.55 eV in the entire range of composition [11], whereas the external quantum efficiency (EQE) measurements implied a minimum gap of 1.36 eV for intermediate *x* compositions and near-linear dependence towards compositional end points [1,3].

In this work, we employ the electroreflectance (ER) spectroscopy at room temperature for characterizing CCZTS thin film solar cell devices with different composition of the absorber layer. Because of its derivative nature and enhanced sensitivity, the ER technique allows accessing and resolving the lowest band gap and high-energy interband electronic transitions in semiconductor materials more precisely than the conventional transmission and reflection methods [12–14]. The effects of Cu off-stoichiometry and Zn alloying of the CCTS absorber layer on the band gap transitions are investigated in detail. Assessing such effects are very important for improving solar cell devices using earth-abundant semiconducting materials [15].

II. EXPERIMENT DETAILS

The $Cu_2(Cd_{1-x}, Zn_x)SnS_4$ absorbers ($x = 0$, 0.4, 0.6, 0.7, 0.8, 1.0) with a thickness of 1 μm were deposited by the spin-coating process on the Mo-coated glass, following the methods described in Ref. [6]. In brief, the spin-coating solution was prepared by dissolving copper acetate monohydrate, zinc acetate dihydrate, cadmium acetate dihydrate, tin chloride dihydrate, and thiourea in the solvent 2-methoxyethanol for 2 h at 50 °C. The clear solution obtained was then spin coated on Mo-glass substrate at 4000 rpm followed by annealing in air at ∼280 °C for 2 min. This spin-coating and annealing step was repeated 13 times. The films were then sulfurized for 40 min in a two-zone furnace in an Ar atmosphere (400-mbar pressure), with temperature of the sample zone maintained at 580–600 °C and that of the sulfur zone maintained at 200 °C. The samples were allowed to cool naturally in the furnace. The solar cell devices were finished by adding a CdS buffer layer using chemical bath deposition (9 min at 80 °C in a solution of 140 ml water, 20 ml

*sergiu.levcenco@uni-leipzig.de

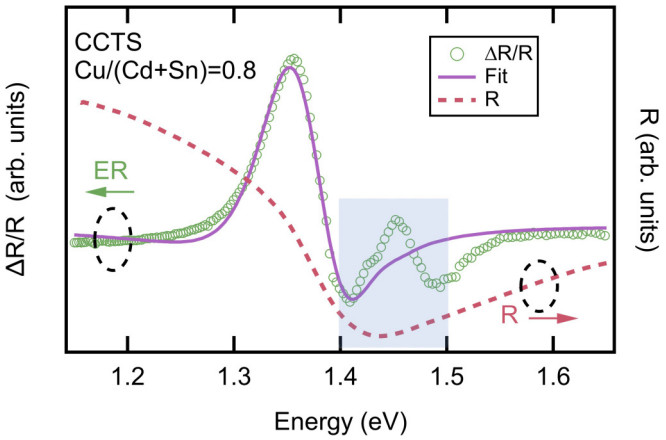

FIG. 1. Room-temperature electroreflectance (green circles) and reflectance (dashed red line) spectra on CCTS sample with $Cu/(Cd + Sn) = 0.8$ composition. The solid line is fit to Eq. (4). The region highlighted with light blue background shows spectral region where the minimum of the reflectance occurs.

0.015 M $CdSO_4$, 20 ml 0.015 M thiourea, and 20 ml of 28–30% ammonia solution) and indium tin oxide (ITO) layer using DC magnetron sputtering (50-W power for 55 min). Note that the ITO layer thickness in this sample series was in the range of 400–500 nm due to batch-to-batch variation. Devices of area 0.16 cm^2 were delineated using mechanical scribing, and Ag was printed on the devices as a top contact. ER experiment on CCZTS devices was conducted on a setup similar to one already described elsewhere [16]. Light from a 150-W halogen lamp passed through a 1/4-m grating monochromator served as the probe beam. A 160-Hz, 1-V peak-to-peak, square wave was used to modulate the electric field across the samples. A dual-phase lock-in was used to extract the modulating part of the reflective signal with a Si photodiode.

III. RESULTS AND DISCUSSION

Figure 1 presents the ER spectrum (shown by the open circles) of CCTS sample with $Cu/(Cd + Sn) = 0.8$ measured in the region of the lowest band gap transitions. A pronounced spectral feature at about 1.35 eV and a weak spectral feature at 1.45 eV are clearly identified. The low-energy feature arises from the band gap transition [5,17]. However, the interpretation of the high-energy feature is more complex and it can be associated with Franz-Keldysh oscillations (FKO) induced by the internal *p-n* junction field [12,13] or with distortion of the ER signal due to interference effect of the window overlayer [14,18] or even to contribution from the high-energy unknown transition. In the case of the interference effect, it has been experimentally demonstrated that different thicknesses of the ZnO:Al window of epitaxial $Cu_2ZnSnSe_4$ thin film solar samples resulted in different shape ER signal in the band-edge region of the absorber layer [19]. To obtain relevant information on the possible origin of the spectral ER signal of CCTS sample, we perform a quantitative analysis based on the ER theory [12,13].

In the ER experiment the relative change of the reflectance is defined as [20]

$$\frac{\Delta R}{R} = \mathrm{Re}[(\alpha - i\beta)(\Delta\varepsilon_1 + i\Delta\varepsilon_2)], \quad (1)$$

where α and β are the Seraphin coefficients, and $\Delta\varepsilon = \Delta\varepsilon_1 + i\Delta\varepsilon_2$ is the change of the complex dielectric function induced by the modulating of the electric field. For a given electromodulation the analytical form of $\Delta\varepsilon$ can be calculated if the dielectric function and the type of critical point are known. Here, we assume a three-dimensional (3D) M_0 critical point (CP) for the lowest band gap transitions in CCTZS and the quantity $\Delta\varepsilon$ can be then obtained as [21]

$$\Delta\varepsilon = B\theta^{0.5}H(z)(E - i\Gamma)^{-2}, \quad (2)$$

with $z = (E_g - E + i\Gamma)/\hbar\theta$, where E_g is the band gap transition energy, E is the photon energy, Γ is the Lorentzian broadening parameter, B is the amplitude related to the transition strength, $\hbar\theta = \sqrt[3]{(\hbar q_e F)^2/2\mu}$ is the electro-optic energy, where F is the amplitude of the electric field strength, q_e is the elementary charge, and μ is the reduced effective mass in the direction of F. $H(z)$ is the electro-optic function expressed for a 3D M_0 CP as [22,23]

$$H(z) = 2\pi\,(e^{-i(\pi/3)}A_i'(z)A_i'(w) + wA_i(z)A_i(w)) + i\sqrt{z}, \quad (3)$$

with $w = ze^{-i(2\pi/3)}$, where $A_i'(z)$ and $A_i'(w)$ denote the first derivatives of the Airy functions of the first kind $A_i(z)$ and $A_i(w)$ of complex argument, respectively.

For the bulk materials and optically thick films in the near band gap region the term $(\alpha - i\beta)$ with the Seraphin coefficients in Eq. (1) can be well approximated by an energy-independent $Ce^{-i\varphi}$ term, and the overall functional form for the relative change of the reflectance can be simply reduced to [12,24]

$$\frac{\Delta R}{R} = \mathrm{Re}[Ce^{i\varphi}H(z)(E - i\Gamma)^{-2}], \quad (4)$$

where the C and φ parameters are redefined to include constant coefficients in Eq. (2). Note that in this approximation one requires no additional information on the dielectric function itself for the material under study. The $\frac{\Delta R}{R}$ quantity thus derived depends on the amplitude C, the phase φ, the electro-optic energy $\hbar\theta$, the broadening Γ, and the band gap E_g parameters. It is worth noting that with increasing ratio of $\hbar\theta/\Gamma$ the FKO signal intensity increases and appears more clear in ER spectrum above the band gap [12,13]. The numerical evaluation of the unknown parameters from the experimental ER data is performed with simulating annealing (SA) algorithm designed for computing the global minimum of the function with multiple local extrema [25]. The application of the SA algorithm to evaluate model parameters for different values of $\hbar\theta/\Gamma$ ratio is exemplified the synthetic ER data with additional random noise to mimic experimental measurement error (Fig. S1 and Table S1 of the Supplemental Material [26]).

The solid line in Fig. 1 shows a SA fit result to Eq. (4) for CCTS sample with $Cu/(Cd + Sn) = 0.8$. We see the deviation of the theoretical curve from the ER data in the whole spectral range. Moreover, the high-energy feature (at 1.45 eV)

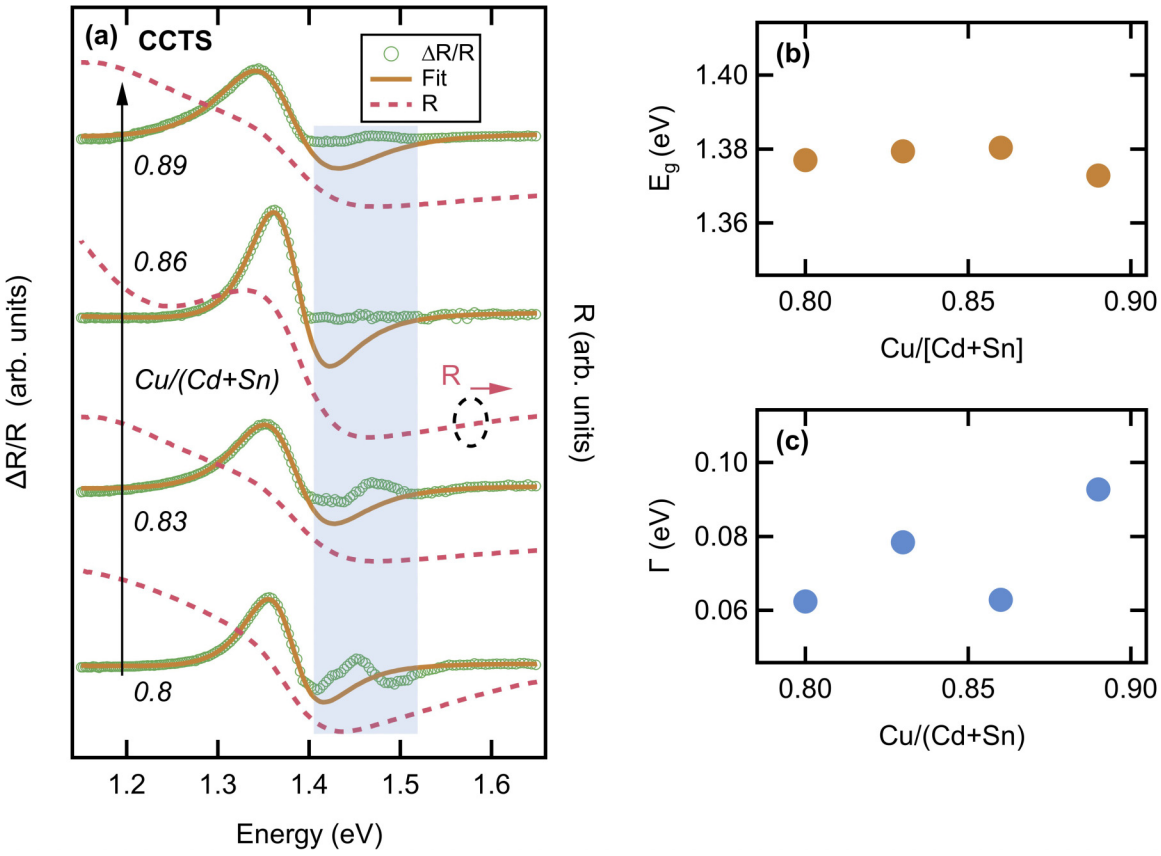

FIG. 2. (a) Room-temperature electroreflectance (green circles) and reflectance (dashed red line) spectra on CCTS sample with varied Cu/(Cd+Sn) composition. For clarity, these optical spectra are vertically shifted. The region highlighted with light blue background shows spectral region where the minimum of the reflectance occurs. The dark orange solid lines are fits to Eq. (4) over the limited range. The evaluated (b) energy and (c) broadening of the band gap transitions as a function of Cu composition.

cannot be modeled with the line shape of FKO structure. However, a closer inspection of reflection (R) spectra measured with a white standard shows a minimum of reflectance in this spectral region, which is additionally highlighted in Fig. 1. This minimum of R is attributed to an interference minimum originating from the top ITO window layer of the CCTS device as the interference effects are best seen in the optical response of the solar cell but not in the as-deposited absorber layer (Fig. S1). The computed R spectra with a matrix method for multilayer structures [27–29] and reasonable assumptions for the optical constants of the individual layers [27,30,31] show also better agreement with the experimental data for the incoherent behavior for the absorber layer and partially coherent behavior [28,29] of the ITO layer (Fig. S2 of the Supplemental Material [26]). Note that the difference in the absolute values between the measured and calculated R spectra is mostly due to light scattering from the rough surfaces of the individual layers that reduce the specular reflection.

It is well known that a distortion of the ER signal for a multilayer system is induced by large fluctuation of the Seraphin coefficients near the interference minimum [18]. In other words, the ER signal in the general equation [Eq. (1)] is mainly determined by the contribution from the Seraphin coefficients and not by the $\Delta\varepsilon$ term. In fact, it can be properly accounted for by using the dielectric function and thickness of each individual layer of the multilayer system and by calculating the dependence of the Seraphin coefficients on photon energy as it was demonstrated on chalcopyrite $Cu(In, Ga)Se_2$ solar cells devices [14] or InGaAs/GaAs/AlAs vertical-cavity surface emitting lasers [32]. Compared to ternary chalcopyrite or III–V compounds, the optical properties of Cd-based kesterites are not understood and in order to calculate the ER signal in a general way based on Eqs. (1)–(3) one first requires the dielectric function study on this semiconductor family. A further complication is the realistic assumption on the interfaces of the considered multilayer system that are not perfectly smooth in the actual polycrystalline solar cells devices. This presents an additional difficulty for the modeling of the reflection spectra on a quantitative level [14]. In what follows, we evaluate the ER model parameters with Eq. (4) using a limited experimental range, excluding the region of reflectance minima where the influence of Seraphin coefficients on ER signal cannot be neglected.

Figure 2(a) illustrates the ER and R spectra on the CCTS samples with different Cu/(Cd+Sn) composition varying from 0.8 to 0.89. The ER spectra produced by additional samples resemble the key characteristics of those found in Fig. 1: the main ER feature at 1.35 eV and the high-energy ER feature at 1.45–1.47 eV. Comparison of ER and R spectra suggests a strong correlation between the high-energy ER feature and the minimum in the reflectance [as highlighted in Fig. 2(a)]. This supports our hypothesis that the high-energy spectral feature

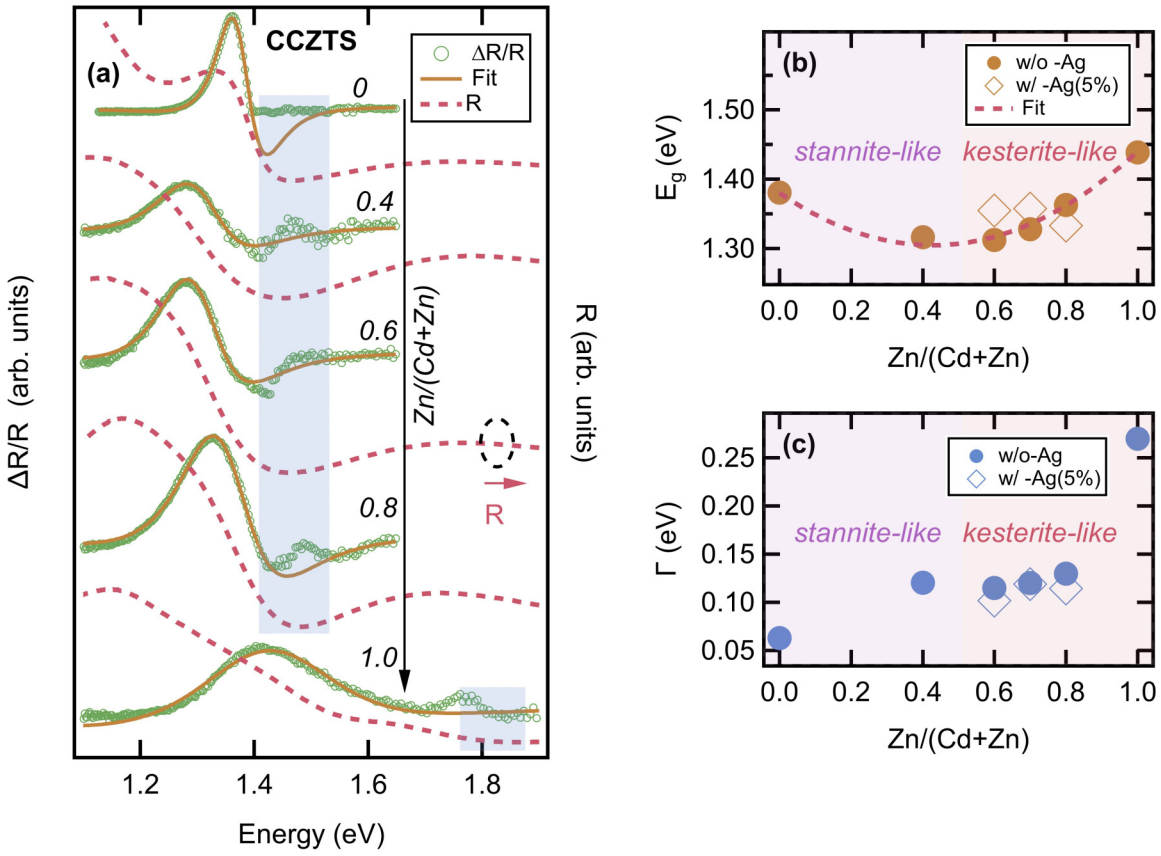

FIG. 3. (a) Room-temperature electroreflectance (green circles) and reflectance (dashed red line) spectra on CCZTS sample with varied Zn/(Cd+Zn) composition. For clarity, these optical spectra are vertically shifted. The region highlighted with light blue color shows region where the minimum of the reflectance occurs. The dark orange solid lines are fits to Eq. (4) over the limited range. The evaluated (b) energy and (c) broadening of the band gap transitions as a function of Zn composition for the CCZTS alloys undoped (closed circles) and 5% Ag-doped (open rhombs).

is due to an interference effect of the ITO window layer and that it is less likely to originate from the unknown high-energy transition. The solid lines in Fig. 2(a) are SA fits to Eq. (4).

The evaluated values of the electro-optic energy are in the range of 10–12 meV. The obtained values of the band gap and broadening parameters are plotted in Figs. 2(b) and 2(c), respectively. It is seen that Γ increases with Cu content by about 30 meV, while E_g is nearly constant. The observed compositional variation of the broadening parameter can be explained by an increase of the formation energy for the $2Cu_{Cd} + Sn_{Cd}$ defect cluster, which gives rise to band gap fluctuations in the Cu_2CdSnS_4 material [5,33]. Our results are in agreement with a previous report on external quantum efficiency from CCTS solar cells [5]. However, a more precise comparison is rather difficult to make as no inclusion of reflectance spectra in the extraction of the absorption coefficient from EQE data was done [34]. Note that our determined value of $E_g = 1.38$ eV is consistent with absorption results on CCTS single crystals [35], EQE on monograin powders [3], and photoluminescence on polycrystalline powders [17]. In contrast to kesterite CZTSSe [36], the CCTS samples display a near-constant E_g over the probed Cu compositional range [Fig. 2(b)], showing evidence of more structural order [37] and possibly a less-pronounced effect of the Cu vacancy on the CCTS valence band [38] compared with kesterite compounds. Note that the broadening parameter of CCTS is also lower by 30–50 meV than the broadening of E_g transitions determined from the ER on CZTSSe polycrystalline thin films [39,40] and hence additionally points to a better crystal quality of CCTS compounds.

Figure 3(a) presents ER and R spectra on the group of CCZTS samples with varied Zn content and nearly constant Cu-poor composition ($Cu/(Zn + Cd + Sn) = 0.86$). The main ER feature related to band gap transitions and the accompanied ER feature at higher energy attributed to the interference effect in the ITO window layer are well resolved in these optical spectra. It can be also observed that the main ER feature exhibits a u-shape behavior with increase of Zn content. The solid lines represent fits of Eq. (4) to the experimental data. The extracted values of the electro-optic energy are about 10-20 meV for these samples. The minimum of the calculated transition energy occurs at $Zn \approx 0.4$–0.6, as shown by the band gap plot in Fig. 3(b), close to the compositional point where the CCZTS structure can be considered a 50:50 solid solution of kesterite-type and stannite-type structures [37]. It has been shown that a continuous structural change from kesterite to stannite occurs as $Cd/(Zn + Cd)$ ratio increases [37]. The determined E_g dependency on Zn composition agrees with the previous reports on thin films [17] and monograins [3], but it is in conflict with the earlier results

on thin films with low Zn composition [11]. In analogy to ternary and multinary compounds, the band gap dependence on the composition x can be expressed with a simple quadratic dependence [41] as

$$E_g(x) = (1-x)E_g(x=0) + xE_g(x=1) - x(1-x)b, \quad (5)$$

where $E_g(x=0)$ and $E_g(x=1)$ correspond to the band gap values in the end points of the multinary alloy and b is the bowing parameter. The least-square fit of our experimental data [Fig. 3(b)] with Eq. (5) yields the value $b = 0.4$ eV. A similar value of the bowing coefficient has been theoretically obtained for $Cu_2Zn(Sn, Si)Se_4$ alloys [42], while bowing coefficients ranging from 0.1 to 0.2 eV in mixed-cation $Cu_2Zn(Sn, Ge)Se_4$ and mixed-anion $Cu_2ZnSn(Se, S)_4$ alloys have been reported [15,43].

The effect of Zn on the broadening parameter is given in Fig. 3(c). Although an appreciable increase of Γ with Zn content is clearly observed, for a wide compositional range ($0.4 < \mathrm{Zn} < 0.8$) the value of Γ parameter is found to be nearly constant: 0.11–0.13 eV. The obtained $\Gamma = 0.27$ eV for the CZTS ($\mathrm{Zn}/(\mathrm{Cd}+\mathrm{Zn}) = 1$) sample is of comparable order to the reported value of 0.2 eV on single crystals [44], meaning a higher disorder effect created by the presence of different cation defects in the crystal lattice of Cd-free sample.

Because the carrier concentration might also influence the broadening parameter [12], we have additionally investigated a second group of CCZTS samples alloyed with 5% Ag. The Hall data indicated a decrease in carrier concentration for this group of samples to values of $2–3 \times 10^{14}$ cm^{-3} [6]. The representative ER and R spectra on 5% Ag CCZTS samples (Fig. S3 of the Supplemental Material [26]) are similar to the first group of CCZTS samples and the evaluated E_g and Γ parameters are additionally included in Figs. 3(a) and 3(b). Only a slight decrease of the Γ parameter by about 10 meV is found for Ag-alloyed samples. Thus, we conclude that the structural disorder mechanism mainly affects the broadening of the band gap transitions in CCZTS alloys.

IV. CONCLUSIONS

To summarize, room-temperature ER is performed to study the band gap transitions of Cu_2CdSnS_4 and $Cu_2(Cd_{1-x}, Zn_x)SnS_4$-based solar cells. We propose that additional reflectance measurements are important and have to be carefully considered in the analysis of distinct ER features from these types of multilayer samples. A detailed line-shape analysis of the ER spectra yields important absorber parameters such as energy and broadening of the band gap transitions as well as reveals the effects of Cu composition and Zn alloying on them. The band gap of Cu_2CdSnS_4 is nearly independent of Cu content, while the broadening parameter apparently varies by about 30 meV. The compositional dependence of the band gap in $Cu_2(Cd_{1-x}, Zn_x)SnS_4$ alloys follows the $E_g(x) = 1.38(1-x) + 1.44x - 0.4x(1-x)$ analytical form. Based on the weak effect of the doping on the ER feature linewidth we suggest that structural disorder is responsible for the broadening of the band gap transitions. The results of our work demonstrate the considerable potential of the ER method in studying and characterizing absorbers in the device architecture.

ACKNOWLEDGMENTS

L.H.W. and S.H. acknowledge the funding support from the CREATE Programme under the Campus for Research Excellence and Technological Enterprise (CREATE), which is supported by the National Research Foundation, Prime Minister's Office, Singapore.

[1] Z. Su, J. M. R. Tan, X. Li, X. Zeng, S. K. Batabyal, and L. H. Wong, Adv. Energy Mater. **5**, 1500682 (2015).
[2] C. Yan, K. Sun, J. Huang, S. Johnston, F. Liu, B. P. Veettil, K. Sun, A. Pu, F. Zhou, J. A. Stride, M. A. Green, and X. Hao, ACS Energy Lett. **2**, 930 (2017).
[3] M. Pilvet, M. Kauk-Kuusik, M. Altosaar, M. Grossberg, M. Danilson, K. Timmo, A. Mere, and V. Mikli, Thin Solid Films **582**, 180 (2015).
[4] S. Wagner and P. M. Bridenbaugh, J. Cryst. Growth **39**, 151 (1977).
[5] S. Hadke, S. Levcenko, G. S. Gautam, C. J. Hages, J. A. Márquez, V. Izquierdo-Roca, E. A. Carter, T. Unold, and L. H. Wong, Adv. Energy Mater. **9**, 1902509 (2019).
[6] S. H. Hadke, S. Levcenko, S. Lie, C. J. Hages, J. A. Márquez, T. Unold, and L. H. Wong, Adv. Energy Mater. **8**, 1802540 (2018).
[7] Z. Su, G. Liang, P. Fan, J. Luo, Z. Zheng, Z. Xie, W. Wang, S. Chen, J. Hu, Y. Wei, C. Yan, J. Huang, X. Hao, and F. Liu, Adv. Mater. **32**, 2000121 (2020).
[8] S. Schorr, G. Gurieva, M. Guc, M. Dimitrievska, A. Pérez-Rodríguez, V. Izquierdo-Roca, C. S. Schnohr, J. Kim, W. Jo, and J. M. Merino, J. Phys. Energy **2**, 012002 (2019).
[9] M. Grossberg, J. Krustok, C. J. Hages, D. Bishop, O. Gunawan, R. Scheer, S. M. Lyam, H. Hempel, S. Levcenko, and T. Unold, J. Phys. Energy **1**, 044002 (2019).
[10] K. Ito and T. Nakazawa, Jpn. J. Appl. Phys. **27**, 2094 (1988).
[11] Z. Y. Xiao, Y. F. Li, B. Yao, R. Deng, Z. H. Ding, T. Wu, G. Yang, C. R. Li, Z. Y. Dong, L. Liu, L. G. Zhang, and H. F. Zhao, J. Appl. Phys. **114**, 183506 (2013).
[12] F. H. Pollak and H. Shen, Mater. Sci. Eng. R. **10**, xv (1993).
[13] D. E. Aspnes, in *Handbook on Semiconductors, Vol. 2: Optical Properties of Semiconductors*, edited by M. Balkanski (North Holland, Amsterdam, 1980), p. 109.
[14] C. Huber, C. Krämmer, D. Sperber, A. Magin, H. Kalt, and M. Hetterich, Phys. Rev. B **92**, 075201 (2015).
[15] S. Adachi, *Earth-abundant Materials for Solar Cells Cu_2-II-IV-VI_4 Semiconductors* (John Wiley & Sons Ltd., West Sussex, 2015).
[16] S. Levcenko, H. Stange, L. Choubrac, D. Greiner, M. D. Heinemann, R. Mainz, and T. Unold, J. Appl. Phys. **127**, 125701 (2020).

[17] M. Pilvet, M. Kauk-Kuusik, M. Grossberg, T. Raadik, V. Mikli, R. Traksmaa, J. Raudoja, K. Timmo, and J. Krustok, J. Alloys Compd. **723**, 820 (2017).
[18] D. E. Aspnes, J. Opt. Soc. Am. **63**, 1380 (1973).
[19] C. Krämmer, C. Huber, A. Redinger, D. Sperber, G. Rey, S. Siebentritt, H. Kalt, and M. Hetterich, Appl. Phys. Lett. **107**, 222104 (2015).
[20] B. O. Seraphin and N. Bottka, Phys. Rev. **145**, 628 (1966).
[21] R. A. Batchelor, A. C. Brown, and A. Hamnett, Phys. Rev. B **41**, 1401 (1990).
[22] D. E. Aspnes, Phys. Rev. **153**, 972 (1967).
[23] J. P. Estrera, W. M. Duncan, and R. Glosser, Phys. Rev. B **49**, 7281 (1994).
[24] D. J. Hall, T. J. C. Hosea, and D. Lancefield, J. Appl. Phys. **82**, 3092 (1997).
[25] A. Corana, M. Marchesi, C. Martini, and S. Ridella, ACM Trans. Math. Software **13**, 262 (1987).
[26] See Supplemental Material at http://link.aps.org/supplemental/10.1103/PhysRevMaterials.5.104605 for synthetic ER data and evaluation of the model parameters with SA algorithm, experimental and calculated reflectance for CCTS sample with $Cu/(Cd + Sn) = 0.8$, and ER and reflectance data of the CCZTS samples alloyed with 5% Ag.
[27] E. Centurioni, Appl. Opt. **44**, 7532 (2005).
[28] M. C. Troparevsky, A. S. Sabau, A. R. Lupini, and Z. Zhang, Opt. Express **18**, 24715 (2010).
[29] R. Santbergen, A. H. M. Smets, and M. Zeman, Opt. Express **21**, A262 (2012).
[30] S. Y. Li, S. Zamulko, C. Persson, N. Ross, J. K. Larsen, and C. Platzer-Björkmann, Appl. Phys. Lett. **110**, 021905 (2017).
[31] J. H. Weaver, D. W. Lynch, and C. G. Olson, Phys. Rev. B **10**, 501 (1974).
[32] P. J. Klar, G. Rowland, P. J. S. Thomas, A. Onischenko, T. E. Sale, T. J. C. Hosea, and R. Grey, Phys. Rev. B **59**, 2894 (1999).
[33] G. Rey, G. Larramona, S. Bourdais, C. Choné, B. Delatouche, A. Jacob, G. Dennler, and S. Siebentritt, Sol. Energy Mater. Sol. Cells **179**, 142 (2018).
[34] X. X. Liu and J. R. Sites, J. Appl. Phys. **75**, 577 (1994).
[35] H. Matsushita, T. Ichikawa, and A. Katsui, J. Mater. Sci. **40**, 2003 (2005).
[36] M. Lang, T. Renz, N. Mathes, M. Neuwirth, T. Schnabel, H. Kalt, and M. Hetterich, Appl. Phys. Lett. **109**, 142103 (2016).
[37] S. Hadke, W. Chen, J. M. R. Tan, M. Guc, V. Izquierdo-Roca, G.-M. Rignanese, G. Hautier, and L. H. Wong, J. Mater. Chem. A **7**, 26927 (2019).
[38] K. Yu and E. A. Carter, Chem. Mater. **28**, 864 (2016).
[39] C. Krämmer, C. Huber, C. Zimmermann, M. Lang, T. Schnabel, T. Abzieher, E. Ahlswede, H. Kalt, and M. Hetterich, Appl. Phys. Lett. **105**, 262104 (2014).
[40] J. Krustok, T. Raadik, M. Grossberg, S. Giraldo, M. Neuschitzer, S. López-Marino, and E. Saucedo, Mater. Sci. Semicond. Process **39**, 251 (2015).
[41] J. A. Van Vechten and T. K. Bergstresser, Phys. Rev. B **1**, 3351 (1970).
[42] Q. Shu, J.-H. Yang, S. Chen, B. Huang, H. Xiang, X. G. Gong, and S.-H. Wei, Phys. Rev. B **87**, 115208 (2013).
[43] S. Chen, A. Walsh, J.-H. Yang, X. G. Gong, L. Sun, P.-X. Yang, J.-H. Chu, and S.-H. Wei, Phys. Rev. B **83**, 125201 (2011).
[44] T. Ming, M. T. Weller, G. P. Kissling, L. M. Peter, P. Dale, F. Babbe, J. de Wild, B. Wenger, H. J. Snaith, and D. Lane, J. Mater. Chem. A **5**, 1192 (2017).